Quench Dynamics and Orthogonality Catastrophe of Bose Polarons

S. I. Mistakidis,[1] G. C. Katsimiga,[1] G. M. Koutentakis,[1,2] Th. Busch,[3] and P. Schmelcher[1,2]
[1]Center for Optical Quantum Technologies, Department of Physics, University of Hamburg, Luruper Chaussee 149, 22761 Hamburg, Germany
[2]The Hamburg Centre for Ultrafast Imaging, Universität Hamburg, Luruper Chaussee 149, 22761 Hamburg, Germany
[3]Quantum Systems Unit, OIST Graduate University, Onna, Okinawa 904-0495, Japan

(Received 26 November 2018; published 8 May 2019)

We monitor the correlated quench induced dynamical dressing of a spinor impurity repulsively interacting with a Bose-Einstein condensate. Inspecting the temporal evolution of the structure factor, three distinct dynamical regions arise upon increasing the interspecies interaction. These regions are found to be related to the segregated nature of the impurity and to the Ohmic character of the bath. It is shown that the impurity dynamics can be described by an effective potential that deforms from a harmonic to a double-well one when crossing the miscibility-immiscibility threshold. In particular, for miscible components the polaron formation is imprinted on the spectral response of the system. We further illustrate that for increasing interaction an orthogonality catastrophe occurs and the polaron picture breaks down. Then a dissipative motion of the impurity takes place leading to a transfer of energy to its environment. This process signals the presence of entanglement in the many-body system.

DOI: 10.1103/PhysRevLett.122.183001

Introduction.—A valuable asset of ultracold atoms is the opportunity to track the real time dynamics of quantum many-body (MB) systems such as multicomponent quantum gases composed of different atomic species [1] or different hyperfine states of the same species [2,3]. In particular, the realization of highly population imbalanced atomic gases with tunable interactions [4–15] has already led to fundamentally new insights regarding Fermi [16–29] and very recently Bose polarons [30–40]. In this latter context the observation of coherent attractive and repulsive quasiparticles [41], even in the strongly interacting regime [42], refueled the scientific interest towards understanding their underlying dynamics.

Most of the theoretical studies regarding Bose polarons have been focused on a mean-field [43–46] description and on the Fröhlich model [47–52]. Only very recently theories going beyond the Fröhlich paradigm [53–59] and including higher-order correlations [60,61] have been developed, thereby allowing for the investigation of Bose polarons also in the intermediate and strong interaction regime. However, current experiments realized both in one [32–34] and three dimensions [41,42] probed the nonequilibrium dynamics of Bose polarons and necessitated the presence of higher-order correlations for an adequate description of the observed dynamics. Thus, the interplay of higher-order correlations during the out-of-equilibrium dynamics of bosonic impurities immersed in a Bose-Einstein condensate (BEC) is a key ingredient for advancing our understanding of the dynamics of such MB systems. On the theoretical side efforts concerning the nonequilibrium dynamics of Bose polarons [62–67] are quite recent and remarkably only a few of them include quantum fluctuations [67–69].

In this Letter, motivated by current experiments [32,41,42,70,71] we explore the interaction quench dynamics of a spinor impurity coupled to a BEC. Focusing on repulsively interacting multicomponent bosonic systems in a one-dimensional (1D) harmonic trap, we showcase the dynamical dressing of the impurity when all particle correlations are taken into account. Three distinct dynamical regions with respect to the interspecies interaction strength are identified and captured by the structure factor, which is the spin polarization (contrast) of the impurity [72]. These regions are shown to be related to the miscible and immiscible character of the system and are indicative of the Ohmic character of the bath [66,73]. Their extent can be manipulated by adjusting the intraspecies repulsion of the BEC alias bath or by changing its particle number, thereby addressing the few to many-body crossover. This tunability is of significant importance since it leads to a longevity of the polaron and thus facilitates the control of quasiparticles. One of our key results consists of the interpretation of the Bose polaron dynamics in terms of an effective potential. The latter is found to be an adequate approximation in the weakly interacting case assuming the Thomas-Fermi approximation for the bath and generalizes the results of Ref. [74]. We demonstrate that deep in the immiscible phase, where entanglement is strong, the Bose polaron ceases to exist due to the orthogonality catastrophe [75,76]. In this strong interaction regime a dissipative motion of the impurity is observed accompanied by the population of several lower-lying excited states of the effective potential.

The latter involves now the single-particle density of the MB bath and provides only a very approximate picture of the impurity dynamics since entanglement is significant. This mechanism of dissipation in turn leads to a transfer of energy from the impurity to its environment also leading to a substantial entanglement in the system.

Model.—We consider a system consisting of a single impurity of mass m_I having an additional spin-1/2 degree of freedom. The impurity is in the superposition $|\Psi_S\rangle = \alpha|\uparrow\rangle + \beta|\downarrow\rangle$, with α, β denoting the different weights used that account for a partial or complete dressing of the single impurity. The impurity is immersed in a 1D harmonically confined BEC of $N_B = 100$ repulsively interacting atoms of mass m_B and trap frequency $\omega_B = \omega_I = 1.0$. The MB Hamiltonian of the system reads

$$\hat{H} = \hat{H}_B^0 + \sum_a \hat{H}_a^0 + \hat{H}_{BB} + \hat{H}_{BI}. \tag{1}$$

Here, $\hat{H}_B^0 = \int dx \hat{\Psi}_B^\dagger(x)[-(\hbar^2/2m_B)(d^2/dx^2) + \frac{1}{2}m_B\omega_B^2 x^2]\hat{\Psi}_B(x)$ is the Hamiltonian describing the motion of the BEC that serves as a bath for the impurity atom. $\hat{H}_a^0 = \int dx \hat{\Psi}_a^\dagger(x)[-(\hbar^2/2m_I)(d^2/dx^2) + \frac{1}{2}m_I\omega_I^2 x^2)\hat{\Psi}_a(x)$ $(a = \{\uparrow, \downarrow\})$ is the corresponding Hamiltonian for the impurity atom. In both cases $\hat{\Psi}_i(x)$ is the bosonic field-operator of either the majority $(i = B)$ or the impurity $(i = a)$ atoms. We focus on the case of equal masses $m_B = m_I = m$ [41]. $\hat{H}_{BB} = g_{BB}\int dx \hat{\Psi}_B^\dagger(x)\hat{\Psi}_B^\dagger(x)\hat{\Psi}_B(x)\hat{\Psi}_B(x)$ accounts for the contact intraspecies interaction of strength $g_{BB} > 0$ in the BEC component. $\hat{H}_{BI} = g_{BI}\int dx \hat{\Psi}_B^\dagger(x)\hat{\Psi}_\uparrow^\dagger(x)\hat{\Psi}_\uparrow(x)\hat{\Psi}_B(x)$ denotes the interaction between the bath and the part of the impurity being in the spin-$\uparrow$ state, characterized by an effective strength $g_{BI} > 0$, while having a noninteracting spin-$\downarrow$ component. Similar setups have been used in the context of fermionic impurities mostly focusing on the attractive side of interactions [77–81]. The multicomponent system is initially prepared in its ground-state configuration for fixed g_{BB} and $g_{BI} = 0$. We note that our results remain valid also for the case of weak interspecies interactions. Such an initial state preparation is experimentally realizable by means of radiofrequency spectroscopy [41,42,55,71,82] and Ramsey interferometry [71].

To derive the nonequilibrium dynamics of the spinor impurity, we use a nonperturbative method, namely, the multilayer multiconfiguration time-dependent Hartree method for atomic mixtures (ML-MCTDHX). Our method rests on expanding the MB wave function with respect to a variationally optimized time-dependent basis that spans the optimal subspace of the Hilbert space at each time instant. Its multilayer ansatz for the total wave function allows us to account for all intra- and interspecies correlations. In our case the latter are found to be more important than the former [83,84].

Our starting point is the ground state, $|\Psi_{BI}^0\rangle$, obeying the eigenvalue equation $(\hat{H} - \hat{H}_{BI})|\Psi_{BI}^0\rangle = E_0|\Psi_{BI}^0\rangle$, with E_0 denoting the corresponding eigenenergy. We then abruptly switch on at $t = 0$ the interspecies repulsion g_{BI}, and let the system evolve dynamically. The MB wave function following the quench reads

$$|\Psi(t)\rangle = \alpha e^{-i\hat{H}t/\hbar}|\Psi_{BI}^0\rangle|\uparrow\rangle + \beta e^{-iE_0t/\hbar}|\Psi_{BI}^0\rangle|\downarrow\rangle. \tag{2}$$

Results and discussion.—To investigate the nonequilibrium dynamics of the spinor impurity we first consider the case where the impurity is in an equal superposition, namely, $\alpha = \beta = (1/\sqrt{2})$, and determine the time evolution of the total spin polarization $|\langle\hat{\mathbf{S}}(t)\rangle| = \sqrt{\langle\hat{S}_x(t)\rangle^2 + \langle\hat{S}_y(t)\rangle^2}$. Here, $\langle\hat{S}_z(t)\rangle = \langle\hat{S}_z(t=0)\rangle = 0$ since $[\hat{S}_z, \hat{H}] = 0$, while $\hat{S}_i = \int dx \sum_{ab}\hat{\Psi}_a^\dagger(x)\sigma_{ab}^i\hat{\Psi}_b(x)$ is the spin operator in the ith direction $(i = x, y, z)$ and σ_{ab}^i are the Pauli matrices. This quantity is directly related to the so-called Ramsey response [71], namely, the structure factor that is the time-dependent overlap between the interacting and the noninteracting states $|\langle\Psi_{BI}^0|e^{iE_0t/\hbar}e^{-i\hat{H}t/\hbar}|\Psi_{BI}^0\rangle|^2 = |\langle\hat{\mathbf{S}}(t)\rangle|^2 = |S(t)|^2$ [72]. $S(t) = |S(t)|e^{i\phi}$, with $\text{atan}\phi = \langle\hat{S}_x\rangle/\langle\hat{S}_y\rangle$, and the Hamiltonian, $\hat{H}$, after the quench, when the impurity is dressed, is given by Eq. (1).

Figures 1(a)–1(c) illustrate the evolution of the structure factor $|S(t)|$ (contrast) upon increasing the interspecies repulsion g_{BI} for different g_{BB} interactions and also for smaller system sizes. In all cases, three distinct dynamical regions can be inferred, namely, R_I, R_{II}, and R_{III}, which,

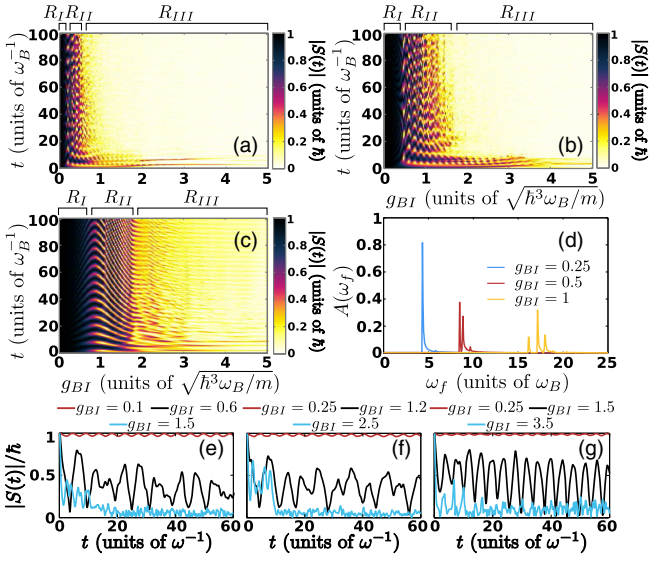

FIG. 1. Evolution of the contrast, $|S(t)|$, upon increasing g_{BI} for (a) $g_{BB} = 0.2$ and (b) $g_{BB} = 0.5$ with $N_B = 100$ and $N_I = 1$. (c) same as (b) but for $N_B = 10$. (d) Excitation spectrum, $A(\omega_f)$, indicating the emergent polaronic peaks for distinct g_{BI} (see legend) and $g_{BB} = 0.5$. (e),(f),(g) illustrate $|S(t)|$ of (a),(b),(c) for different g_{BI} (see legend).

e.g., for $g_{BB} = 0.5$ correspond to $0 \leq g_{BI}^{R_I} < 0.5$, $0.5 \leq g_{BI}^{R_{II}} < 1.65$, and $1.65 \leq g_{BI}^{R_{III}} < 5.0$, respectively. For short times a descent of $|S(t)|$ is observed [71,104]; see Figs. 1(e)–1(g), being sharper for larger g_{BI}. This descent occurs independently of the value of the intraspecies repulsion g_{BB}, compare Figs. 1(e) and 1(f). For larger evolution times $|S(t)|$ performs oscillations that become more pronounced upon increasing g_{BI} within R_I and exhibit a decaying amplitude in R_{II}. In contrast, entering R_{III} $|S(t)|$ exhibits an exponential decay indicating the orthogonality catastrophe. The degree of damping of $|S(t)|$ within R_I, R_{II}, and R_{III} is indicative of a sub-Ohmic, Ohmic, and super-Ohmic behavior of the bath, respectively (see also below). Comparing the temporal evolution of $|S(t)|$ for $g_{BB} = 0.2$ [Fig. 1(a)] to the one for $g_{BB} = 0.5$ [Fig. 1(b)] we observe that the extent of the above-mentioned dynamical regions (R_I, R_{II}, R_{III}) can be manipulated by adjusting g_{BB}. In particular, for larger g_{BB} an enhanced region of finite contrast that enters deeper into the regime of repulsive interspecies interactions can be achieved. This behavior is supported upon decreasing the number of bath particles to $N_B = 10$ [Fig. 1(c)]. In the latter few-body scenario coherent oscillations of $|S(t)|$ are observed [see Fig. 1(c) for $0.8 < g_{BI} < 1.8$] leading to a smoothly decreasing contrast as g_{BI} increases [105]. The aforementioned dynamics takes equally place when the initial superposition state of the spinor impurity involves different weights for each spinor component. This fact can be understood by analytically calculating $|\langle\hat{\mathbf{S}}(t)\rangle|_{\alpha,\beta}$ when considering different weights α and β. Indeed, it holds $|\langle\hat{\mathbf{S}}(t)\rangle|_{\alpha,\beta} = \sqrt{4\alpha^2\beta^2|S(t)|^2 + (|\alpha|^2 - |\beta|^2)^2}$, where $|S(t)|$ stems from the case $\alpha = \beta = 1/\sqrt{2}$.

As expected, the energy spectrum of the impurity is changed upon applying an interaction quench [81]. To quantify this we determine the Fourier transform of $S(t)$. At low impurity densities and weak interspecies interactions $S(t)$ is known to be proportional to the so-called spectral function of quasiparticles $A(\omega_f) = (1/\pi)\mathrm{Re}\{\int_0^\infty dt e^{i\omega_f t} S(t)\}$ [71,72,81,106]. Figure 1(d) illustrates $A(\omega)$ for different interspecies repulsions ranging from small ($g_{BI}^{R_I} = 0.25$) to intermediate ($g_{BI}^{R_{II}} = 0.5$) and large ($g_{BI}^{R_{II}} = 1.0$) interactions, respectively. The observed peak at small g_{BI} located at $\omega = 4.435$ corresponds to the long-time evolution of a well-defined repulsive Bose polaron. In R_{II} two dominant peaks are imprinted in $A(\omega_f)$ centered at $\omega_1 = 8.482$ and $\omega_2 = 8.859$, respectively. These two peaks correspond to a well-defined quasiparticle dressed, for higher frequencies, by higher-order excitations of the BEC. Figures 2(a) and 2(c) depict the evolution of the impurity's one-body density, $\rho_\uparrow^{(1)}(x) = \langle\Psi(t)|\hat{\Psi}_\uparrow^\dagger(x)\hat{\Psi}_\uparrow(x)|\Psi(t)\rangle$, for small and intermediate values of g_{BI}. The observed out-of-equilibrium dynamics of the spinor impurity in both regions R_I and R_{II}

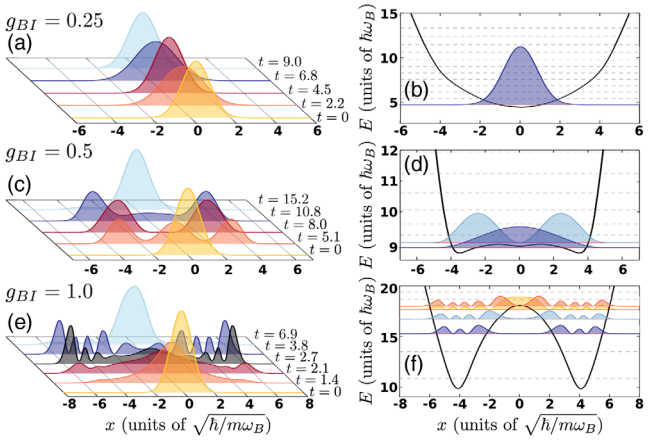

FIG. 2. Selected time instants during evolution of the impurity's one-body density for (a) $g_{BI} = 0.25$, (c) $g_{BI} = 0.5$, and (e) $g_{BI} = 1.0$ illustrating its dynamical dressing. Effective potential and example densities of the corresponding impurity eigenstates for the aforementioned (b) small, (d) intermediate, and (f) large g_{BI} values. Notice that the eigenenergies of V_{eff} are slightly shifted with respect to the polaronic energies obtained within the MB approach [see also Fig. 1(d) and the discussion in the main text]. In all cases dashed gray lines correspond to the energy levels of the effective potential.

can be well approximated by the dynamics in an effective potential. The latter is obtained by considering the bosonic bath as a static potential superimposed to the external harmonic trapping of the impurity, namely,

$$V_{\mathrm{eff}} = \frac{1}{2} m_B \omega_B^2 x^2 + g_{BI}\rho_B^{(1)}(x), \tag{3}$$

where $\rho_B^{(1)}(x)$ is the single-particle density of the BEC at $t = 0$. It is important to stress that V_{eff} does not take into account the renormalization of the quasiparticle's zero-point energy occurring due to its dressing by the bath [68]. This deficit, however, shifts the eigenspectrum of the impurity in a homogeneous manner and, consequently, does not affect its dynamics. For small g_{BI} and fixed g_{BB} the Thomas-Fermi approximation, i.e., $\rho_B^{(1)}(x) = (1/g_{BB})(\mu_B - \frac{1}{2} m_B \omega_B^2 x_B^2)$ with μ_B being the chemical potential of the bath, is valid and $V_{\mathrm{eff}} = \frac{1}{2} m_B \tilde{\omega}_B^2 x^2 + c$. Then V_{eff} is a parabola shifted by $c \equiv (g_{BI}/g_{BB})\mu_B$ possessing a modified trapping frequency [74], $\tilde{\omega}_B^2 \equiv [1 - (g_{BI}/g_{BB})]\omega_B^2 < \omega_B^2$ [see Fig. 2(b)]. In this case the impurity undergoes a breathing motion [Fig. 2(a)]. Note that the notion of V_{eff} can be extended to higher dimensions. However, relying solely on this approximation we can assess only the frequencies of the emergent dynamical modes i.e., the breathing mode, see also Ref. [84]. Contrary to this an increase of g_{BI} such that $g_{BI} > g_{BB}$ changes this effective potential picture. In this case the system enters the immiscible regime and the initial state involves higher-order excitations in the effective potential due to the stronger interaction of the impurity with the bosonic bath

[Fig. 2(c)]. For these intermediate g_{BI} interactions the impurity density develops a two-hump structure being pushed towards the boundaries of the bath and favoring a phase-separated state with the BEC that resides around the trap center (see the discussion below). It is for these intermediate values, indicating a miscible to an immiscible phase transition, that $V_{\rm eff}(x)$ begins to deform into a double-well potential [Fig. 2(d)]. The impurity state corresponds then to the ground or the first excited state of this effective potential. Further increase of g_{BI} leads to the appearance of three dominant peaks in the impurity's excitation spectrum. These peaks are centered at $\omega_3 = 16.15$, $\omega_4 = 17.15$, and $\omega_5 = 17.97$, respectively [Fig. 1(d)], and correspond to even higher excited states of the quasiparticle. The relevant dynamical evolution of the impurity [Fig. 2(e)] showcases the deformation of its one-body density, with these higher excited states occupying the third up to sixth excited state of $V_{\rm eff}$ [Fig. 2(f)]. Entering deeper into the immiscible phase [Fig. 1(b)] results in a fast decay of the contrast at short timescales. Consequently, there is no clear polaronic signature in the relevant excitation spectrum, but rather a multitude of states are occupied in this effective double-well picture. This behavior is caused by the dissipative motion of the impurity leading to a partial transfer of its energy to the bath as we shall argue below.

To deepen our understanding of the dynamics of the spinor impurity we next examine the degree of miscibility between the spin components captured by the overlap integral

$$\Lambda^{\uparrow\downarrow}(t) = \frac{\left[\int dx \rho^{(1)}_{\uparrow}(x,t)\rho^{(1)}_{\downarrow}(x,t)\right]^2}{\int dx (\rho^{(1)}_{\uparrow}(x,t))^2 \int dx (\rho^{(1)}_{\downarrow}(x,t))^2}. \quad (4)$$

Here, e.g., the one-body density of the spin-$\downarrow$ is $\rho^{(1)}_{\downarrow}(x,t) = \langle \Psi(t)|\Psi^{\dagger}_{\downarrow}(t)\Psi_{\downarrow}(t)|\Psi(t)\rangle$. $\Lambda^{\uparrow\downarrow}(t)$ takes values within the interval [0, 1] with zero (unity) denoting the phase immiscible (miscible) spin components. Evidently, the three distinct dynamical regions captured by $|S(t)|$ leave their fingerprints in $\Lambda^{\uparrow\downarrow}(t)$ [Fig. 3(a)]. Note here that $\rho^{(1)}_{\downarrow}(x,t) = \rho^{(1)}_{\uparrow}(x,0)$ and, therefore, $\Lambda^{\uparrow\downarrow}(t)$ is directly related to the contrast [see Fig. 1(b)]. Indeed, within R_I the spin components are maximally miscible, while within R_{II} they oscillate between miscibility and immiscibility. Finally, when the orthogonality catastrophe takes place in R_{III} they become immiscible. This spin segregation, in R_{III}, is manifested in the spatiotemporal evolution of $\rho^{(1)}_{\uparrow}(x,t)$ [Fig. 3(b)] [107]. Evidently, $\rho^{(1)}_{\uparrow}(x,t)$ breaks into two density fragments that perform damped oscillations symmetrically placed around the edges of the Thomas Fermi radius of the bath. These damped oscillations essentially indicate that the spin-$\uparrow$ impurity is initially in a highly excited state of $V_{\rm eff}(x)$ [see Fig. 3(e) for t_1] while

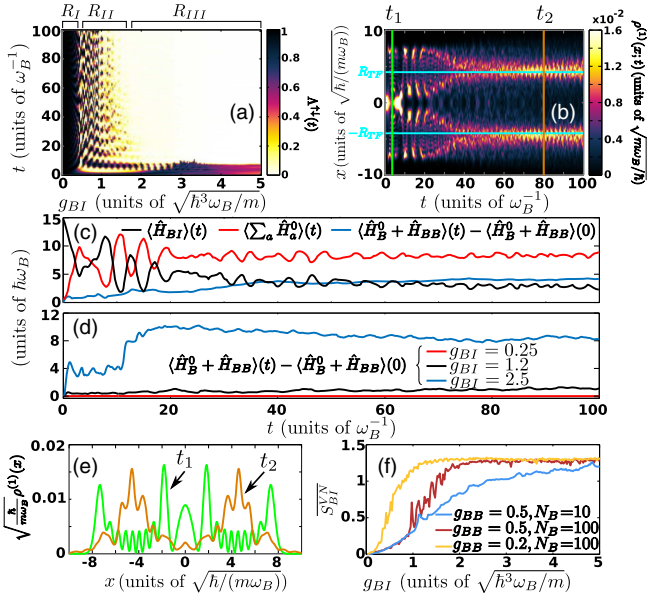

FIG. 3. (a) Evolution of the overlap $\Lambda^{\uparrow\downarrow}(t)$ between the spin-$\uparrow$ and spin-$\downarrow$ states of the impurity atom. (b) One-body density evolution of the spin-$\uparrow$ atom. Horizontal solid lines indicate the position of the Thomas Fermi radius of the bath. (c) Expectation value of the energy (see legend). In both (b),(c) $g_{BI} = 1.7$. (d) Expectation value of the energy of the bath for different g_{BI} (see legend). (e) Density profiles at the time instants marked by the vertical solid lines in (b). (f) Time average of the von-Neumann entropy, $\bar{S}^{VN}_{BI}$, for increasing g_{BI}. In all cases $N_B = 100$, $N_I = 1$, and $g_{BB} = 0.5$.

for later times, e.g., t_2, it populates a superposition of lower excited states. We remark here that $\rho^{(1)}_{\uparrow}(x,t)$ depicted in Fig. 3(e) is obtained from the correlated MB calculation while the interpretation in terms of $V_{\rm eff}$ provides an approximate picture of the impurity dynamics for these strong interactions. The latter behavior implies a transfer of energy from the impurity to the BEC environment [Fig. 3(c)] that is beyond the single-particle dynamics provided via $V_{\rm eff}$. This energy transfer possesses contributions of different magnitude from each term of the above-mentioned superposition leading to different excitations of the BEC and hence it constitutes a manifestation of the entanglement present in the MB system. Since the kinetic energy of the impurity increases during evolution also an increase of its noninteracting energy $\langle\sum_a \hat{H}^0_a\rangle$ is observed. Contrary to this excess of energy, a decrease of the interaction energy $\langle\hat{H}_{BI}\rangle$ occurs since the impurity is expelled to the edges of the BEC, where $\rho^{(1)}_B(x) \ll \rho^{(1)}_B(0)$. Indeed, $\langle\hat{H}^0_B + \hat{H}_{BB}\rangle$ increases in the course of the dynamics capturing the transfer of energy from the impurity to the bath. This dissipation mechanism becomes pronounced within R_{III}. Figure 3(d) shows $\langle\hat{H}^0_B + \hat{H}_{BB}\rangle$ during evolution for different g_{BI}. It becomes evident that within R_I the impurity does not dissipate energy to the bath since the

energy of the latter remains almost constant. However, within the region R_{II} the impurity starts to dissipate energy to the bath and this dissipation rate becomes maximal within R_{III}. This observation further supports the sub-Ohmic, Ohmic, and super-Ohmic behavior of the bath in the different regions. Moreover, to directly expose the presence of entanglement with respect to g_{BI} we invoke the von-Neumann entropy, $S^{VN}_{BI}(t) = -\sum_i \lambda_i(t) \log \lambda_i(t)$ [108]. Note that λ_i's are the eigenvalues of the N_B-body density matrix $\rho_B^{(N_B)} = -\mathrm{Tr}_I[|\Psi(t)\rangle\langle\Psi(t)|]$. Indeed, the time average $\bar{S}^{VN}_{BI}$ [Fig. 3(f)] shows that the dressed impurity is entangled with the BEC within the regions R_I and R_{II}. By inspecting $\bar{S}^{VN}_{BI}$ we observe that its slope becomes maximal in R_{II} and therefore the same holds for the generation of entanglement, see also Ref. [84]. Most importantly the system becomes strongly entangled within R_{III}, where the polaron ceases to exist, showcasing a plateau of $\bar{S}^{VN}_{BI}(t) \approx 1.2$ for fixed $g_{BB} = 0.5$ and for all $g_{BI} \gtrsim 1.65$.

Conclusions.—The correlated quench-induced dynamics of a trapped spinor impurity repulsively interacting with a BEC has been investigated. Inspecting the evolution of the spin polarization reveals three distinct dynamical regions with respect to the interspecies interaction strength. These regions are inherently related to the segregated nature of the multicomponent system and can be tuned by changing the intraspecies repulsion of the BEC or its particle number thereby addressing the few to many-body crossover. Within these three regions the birth, dynamical deformation, and death (orthogonality catastrophe) of the Bose polaron are unraveled. To interpret the impurity dynamics, an effective potential is derived being an adequate approximation for weak interspecies repulsions. For strong repulsions the system is strongly entangled and the impurity's motion becomes dissipative, transferring a part of its energy to the bath while being pushed to the edges of the BEC. Our results pave the way for manipulating the quasiparticle dynamics. An intriguing perspective for future endeavors is to consider more than one impurity where induced interactions can play an important role.

S. I. M. and P. S. gratefully acknowledge financial support by the Deutsche Forschungsgemeinschaft (DFG) in the framework of the SFB 925 "Light induced dynamics and control of correlated quantum systems." G. M. K and P. S. acknowledge the support by the excellence cluster "The Hamburg Center for Ultrafast Imaging: Structure, Dynamics and Control of Matter at the Atomic Scale" of the DFG. This work was also supported by the OIST Graduate University.

G. C. K, S. I. M., and G. M. K. contributed equally to this work.

[1] G. Modugno, M. Modugno, F. Riboli, G. Roati, and M. Inguscio, Phys. Rev. Lett. **89**, 190404 (2002).
[2] C. J. Myatt, E. A. Burt, R. W. Ghrist, E. A. Cornell, and C. E. Wieman, Phys. Rev. Lett. **78**, 586 (1997).
[3] J. Stenger, S. Inouye, D. M. Stamper-Kurn, H.-J. Miesner, A. P. Chikkatur, and W. Ketterle, Nature (London) **396**, 345 (1998).
[4] C.-H. Wu, J. W. Park, P. Ahmadi, S. Will, and M. W. Zwierlein, Phys. Rev. Lett. **109**, 085301 (2012).
[5] M.-S. Heo, T. T. Wang, C. A. Christensen, T. M. Rvachov, D. A. Cotta, J.-H. Choi, Y.-R. Lee, and W. Ketterle, Phys. Rev. A **86**, 021602(R) (2012).
[6] T. D. Cumby, R. A. Shewmon, M.-G. Hu, J. D. Perreault, and D. S. Jin, Phys. Rev. A **87**, 012703 (2013).
[7] G. Roati, M. Zaccanti, C. D'Errico, J. Catani, M. Modugno, A. Simoni, M. Inguscio, and G. Modugno, Phys. Rev. Lett. **99**, 010403 (2007).
[8] K. Pilch, A. D. Lange, A. Prantner, G. Kerner, F. Ferlaino, H.-C. Nägerl, and R. Grimm, Phys. Rev. A **79**, 042718 (2009).
[9] A. Schirotzek, C.-H. Wu, A. Sommer, and M. W. Zwierlein, Phys. Rev. Lett. **102**, 230402 (2009).
[10] C. Kohstall, M. Zaccanti, M. Jag, A. Trenkwalder, P. Massignan, G. M. Bruun, F. Schreck, and R. Grimm, Nature (London) **485**, 615 (2012).
[11] M. Koschorreck, D. Pertot, E. Vogt, B. Fröhlich, M. Feld, and M. Köhl, Nature (London) **485**, 619 (2012).
[12] Y. Zhang, W. Ong, I. Arakelyan, and J. E. Thomas, Phys. Rev. Lett. **108**, 235302 (2012).
[13] N. Spethmann, F. Kindermann, S. John, C. Weber, D. Meschede, and A. Widera, Phys. Rev. Lett. **109**, 235301 (2012).
[14] F. Scazza, G. Valtolina, P. Massignan, A. Recati, A. Amico, A. Burchianti, C. Fort, M. Inguscio, M. Zaccanti, and G. Roati, Phys. Rev. Lett. **118**, 083602 (2017).
[15] N. J. Robinson, J. S. Caux, and R. M. Konik, Phys. Rev. Lett. **116**, 145302 (2016).
[16] S. Nascimbène, N. Navon, K. J. Jiang, L. Tarruell, M. Teichmann, J. McKeever, F. Chevy, and C. Salomon, Phys. Rev. Lett. **103**, 170402 (2009).
[17] M. Punk, P. T. Dumitrescu, and W. Zwerger, Phys. Rev. A **80**, 053605 (2009).
[18] F. Chevy and C. Mora, Rep. Prog. Phys. **73**, 112401 (2010).
[19] X. Cui and H. Zhai, Phys. Rev. A **81**, 041602(R) (2010).
[20] S. Pilati, G. Bertaina, S. Giorgini, and M. Troyer, Phys. Rev. Lett. **105**, 030405 (2010).
[21] P. Massignan and G. Bruun, Eur. Phys. J. D **65**, 83 (2011).
[22] R. Schmidt and T. Enss, Phys. Rev. A **83**, 063620 (2011).
[23] R. Schmidt, T. Enss, V. Pietilä, and E. Demler, Phys. Rev. A **85**, 021602(R) (2012).
[24] V. Ngampruetikorn, J. Levinsen, and M. M. Parish, Europhys. Lett. **98**, 30005 (2012).
[25] P. Massignan, Z. Yu, and G. M. Bruun, Phys. Rev. Lett. **110**, 230401 (2013).
[26] P. Massignan, M. Zaccanti, and G. M. Bruun, Rep. Prog. Phys. **77**, 034401 (2014).
[27] R. Schmidt, M. Knap, D. A. Ivanov, J.-S. You, M. Cetina, and E. Demler, Rep. Prog. Phys. **81**, 024401 (2018).
[28] E. Burovski, V. Cheianov, O. Gamayun, and O. Lychkovskiy, Phys. Rev. A **89**, 041601(R) (2014).

[29] O. Gamayun, O. Lychkovskiy, E. Burovski, M. Malcomson, V. V. Cheianov, and M. B. Zvonarev, Phys. Rev. Lett. **120**, 220605 (2018).
[30] S. Palzer, C. Zipkes, C. Sias, and M. Köhl, Phys. Rev. Lett. **103**, 150601 (2009).
[31] J. Tempere, W. Casteels, M. K. Oberthaler, S. Knoop, E. Timmermans, and J. T. Devreese, Phys. Rev. B **80**, 184504 (2009).
[32] J. Catani, G. Lamporesi, D. Naik, M. Gring, M. Inguscio, F. Minardi, A. Kantian, and T. Giamarchi, Phys. Rev. A **85**, 023623 (2012).
[33] T. Fukuhara, A. Kantian, M. Endres, M. Cheneau, P. Schauss, S. Hild, D. Bellem, U. Schollwöck, T. Giamarchi, C. Gross, I. Bloch, and S. Kuhr, Nat. Phys. **9**, 235 (2013).
[34] R. Scelle, T. Rentrop, A. Trautmann, T. Schuster, and M. K. Oberthaler, Phys. Rev. Lett. **111**, 070401 (2013).
[35] R. Schmidt, H. R. Sadeghpour, and E. Demler, Phys. Rev. Lett. **116**, 105302 (2016).
[36] L. A. Peña Ardila and S. Giorgini, Phys. Rev. A **94**, 063640 (2016).
[37] F. Grusdt, R. Schmidt, Y. E. Shchadilova, and E. Demler, Phys. Rev. A **96**, 013607 (2017).
[38] A. G. Volosniev and H.-W. Hammer, Phys. Rev. A **96**, 031601(R) (2017).
[39] N. E. Guenther, P. Massignan, M. Lewenstein, and G. M. Bruun, Phys. Rev. Lett. **120**, 050405 (2018).
[40] D. Mayer, F. Schmidt, D. Adam, S. Haupt, J. Koch, T. Lausch, J. Nettersheim, Q. Bouton, and A. Widera, J. Phys. B **52**, 015301 (2019).
[41] N. B. Jørgensen, L. Wacker, K. T. Skalmstang, M. M. Parish, J. Levinsen, R. S. Christensen, G. M. Bruun, and J. J. Arlt, Phys. Rev. Lett. **117**, 055302 (2016).
[42] M.-G. Hu, M. J. Van de Graaff, D. Kedar, J. P. Corson, E. A. Cornell, and D. S. Jin, Phys. Rev. Lett. **117**, 055301 (2016).
[43] G. E. Astrakharchik and L. P. Pitaevskii, Phys. Rev. A **70**, 013608 (2004).
[44] F. M. Cucchietti and E. Timmermans, Phys. Rev. Lett. **96**, 210401 (2006).
[45] R. M. Kalas and D. Blume, Phys. Rev. A **73**, 043608 (2006).
[46] M. Bruderer, A. Klein, S. R. Clark, and D. Jaksch, Europhys. Lett. **82**, 30004 (2008).
[47] K. Sacha and E. Timmermans, Phys. Rev. A **73**, 063604 (2006).
[48] M. Bruderer, A. Klein, S. R. Clark, and D. Jaksch, Phys. Rev. A **76**, 011605(R) (2007).
[49] A. Privitera and W. Hofstetter, Phys. Rev. A **82**, 063614 (2010).
[50] W. Casteels, J. Tempere, and J. T. Devreese, Phys. Rev. A **86**, 043614 (2012).
[51] W. Casteels, J. Tempere, and J. T. Devreese, Phys. Rev. A **88**, 013613 (2013).
[52] B. Kain and H. Y. Ling, Phys. Rev. A **94**, 013621 (2016).
[53] W. Li and S. Das Sarma, Phys. Rev. A **90**, 013618 (2014).
[54] L. A. Peña Ardila and S. Giorgini, Phys. Rev. A **92**, 033612 (2015).
[55] Y. E. Shchadilova, R. Schmidt, F. Grusdt, and E. Demler, Phys. Rev. Lett. **117**, 113002 (2016).
[56] S. P. Rath and R. Schmidt, Phys. Rev. A **88**, 053632 (2013).
[57] F. Grusdt, G. E. Astrakharchik, and E. Demler, New J. Phys. **19**, 103035 (2017).
[58] X. Li, G. Bighin, E. Yakaboylu, and M. Lemeshko, Mol. Phys., 1 (2019).
[59] B. Kain and H. Y. Ling, Phys. Rev. A **98**, 033610 (2018).
[60] J. Levinsen, M. M. Parish, and G. M. Bruun, Phys. Rev. Lett. **115**, 125302 (2015).
[61] R. S. Christensen, J. Levinsen, and G. M. Bruun, Phys. Rev. Lett. **115**, 160401 (2015).
[62] M. B. Zvonarev, V. V. Cheianov, and T. Giamarchi, Phys. Rev. Lett. **99**, 240404 (2007).
[63] J. Bonart and L. F. Cugliandolo, Phys. Rev. A **86**, 023636 (2012).
[64] J. Bonart and L. F. Cugliandolo, Europhys. Lett. **101**, 16003 (2013).
[65] A. G. Volosniev, H.-W. Hammer, and N. T. Zinner, Phys. Rev. A **92**, 023623 (2015).
[66] A. Lampo, S. H. Lim, M. Á. García-March, and M. Lewenstein, Quantum **1**, 30 (2017).
[67] F. Grusdt, K. Seetharam, Y. Shchadilova, and E. Demler, Phys. Rev. A **97**, 033612 (2018).
[68] S. I. Mistakidis, A. G. Volosniev, N. T. Zinner, and P. Schmelcher, arXiv:1809.01889.
[69] M. Drescher, M. Salmhofer, and T. Enss, Phys. Rev. A **99**, 023601 (2019).
[70] M. Cetina, M. Jag, R. S. Lous, J. T. M. Walraven, R. Grimm, R. S. Christensen, and G. M. Bruun, Phys. Rev. Lett. **115**, 135302 (2015).
[71] M. Cetina, M. Jag, R. S. Lous, I. Fritsche, J. T. M. Walraven, R. Grimm, J. Levinsen, M. M. Parish, R. Schmidt, M. Knap, and E. Demler, Science **354**, 96 (2016).
[72] M. Knap, A. Shashi, Y. Nishida, A. Imambekov, D. A. Abanin, and E. Demler, Phys. Rev. X **2**, 041020 (2012).
[73] J. Bonart and L. F. Cugliandolo, Phys. Rev. A **86**, 023636 (2012).
[74] A. Sartori and A. Recati, Eur. Phys. J. D **67**, 260 (2013).
[75] P. W. Anderson, Phys. Rev. Lett. **18**, 1049 (1967).
[76] J. Goold, T. Fogarty, N. Lo Gullo, M. Paternostro, and T. Busch, Phys. Rev. A **84**, 063632 (2011).
[77] F. Chevy, Phys. Rev. A **74**, 063628 (2006).
[78] R. Combescot, A. Recati, C. Lobo, and F. Chevy, Phys. Rev. Lett. **98**, 180402 (2007).
[79] R. Combescot and S. Giraud, Phys. Rev. Lett. **101**, 050404 (2008).
[80] R. Combescot, S. Giraud, and X. Leyronas, Europhys. Lett. **88**, 60007 (2009).
[81] M. M. Parish and J. Levinsen, Phys. Rev. B **94**, 184303 (2016).
[82] S. I. Mistakidis, G. C. Katsimiga, G. M. Koutentakis, and P. Schmelcher, New J. Phys. **21**, 043032 (2019).
[83] L. Cao, V. Bolsinger, S. I. Mistakidis, G. M. Koutentakis, S. Krönke, J. M. Schurer, and P. Schmelcher, J. Chem. Phys. **147**, 044106 (2017).
[84] See Supplemental Material at http://link.aps.org/supplemental/10.1103/PhysRevLett.122.183001 for the description of (i) impurity's breathing dynamics; (ii) the effective mass of the polaron; (iii) the ML-MCTDHX

method, and (iv) the entanglement generation, which includes Refs. [86–104].
[85] P. Siegl, S. I. Mistakidis, and P. Schmelcher, Phys. Rev. A **97**, 053626 (2018).
[86] G. M. Koutentakis, S. I. Mistakidis, and P. Schmelcher, Phys. Rev. A **95**, 013617 (2017).
[87] J. P. Ronzheimer, M. Schreiber, S. Braun, S. S. Hodgman, S. Langer, I. P. McCulloch, F. Heidrich-Meisner, I. Bloch, and U. Schneider, Phys. Rev. Lett. **110**, 205301 (2013).
[88] J. W. Abraham and M. Bonitz, Contrib. Plasma Phys. **54**, 27 (2014).
[89] L. Cao, S. Krönke, O. Vendrell, and P. Schmelcher, J. Chem. Phys. **139**, 134103 (2013).
[90] G. C. Katsimiga, G. M. Koutentakis, S. I. Mistakidis, P. G. Kevrekidis, and P. Schmelcher, New J. Phys. **19**, 073004 (2017).
[91] S. I. Mistakidis, G. C. Katsimiga, P. G. Kevrekidis, and P. Schmelcher, New J. Phys. **20**, 043052 (2018).
[92] M. Roncaglia, A. Montorsi, and M. Genovese, Phys. Rev. A **90**, 062303 (2014).
[93] G. M. Koutentakis, S. I. Mistakidis, and P. Schmelcher, New J. Phys., https://doi.org/10.1088/1367-2630/ab14ba (2019).
[94] J. Erdmann, S. I. Mistakidis, and P. Schmelcher, Phys. Rev. A **99**, 013605 (2019).
[95] J. Frenkel, *Wave Mechanics*, 1st ed. (Clarendon Press, Oxford, 1934), pp. 423–428.
[96] P. A. Dirac, Proc. Cambridge Philos. Soc. **26**, 376 (1930).
[97] L. P. Pitaevskii and S. Stringari, *Bose-Einstein Condensation* (Oxford University Press, Oxford, 2003).
[98] P. G. Kevrekidis, D. J. Frantzeskakis, and R. Carretero-González, *The Defocusing Nonlinear Schrödinger Equation* (SIAM, Philadelphia, 2015).
[99] M. Naraschewski and R. J. Glauber, Phys. Rev. A **59**, 4595 (1999).
[100] E. J. Mueller, T. L. Ho, M. Ueda, and G. Baym, Phys. Rev. A **74**, 033612 (2006).
[101] O. Penrose and L. Onsager, Phys. Rev. **104**, 576 (1956).
[102] P. Jain and M. Boninsegni, Phys. Rev. A **83**, 023602 (2011).
[103] S. Bandyopadhyay, A. Roy, and D. Angom, Phys. Rev. A **96**, 043603 (2017).
[104] R. A. Jalabert and H. M. Pastawski, Adv. Solid State Phys. **41**, 483 (2001).
[105] Within the mean-field approximation for both $N_B = 100$ and $N_B = 10$ cases, $|S(t)|$ remains finite for $0 < g_{BI} < 5$ and thus the orthogonality catastrophe as captured by the contrast is absent.
[106] P. Nozières and C. T. De Dominicis, Phys. Rev. **178**, 1097 (1969).
[107] The spin-$\downarrow$ component, being noninteracting, remains around the trap center for all times.
[108] R. Horodecki, P. Horodecki, M. Horodecki, and K. Horodecki, Rev. Mod. Phys. **81**, 865 (2009).